JCP, in press, doi:10.1063/1.4864657

Oxygen diffusion and reactivity at low temperature on bare amorphous olivine-type silicate

M. Minissale,[1, a)] E. Congiu,[1] and F. Dulieu[1]

LERMA-LAMAp, Université de Cergy-Pontoise, Observatoire de Paris, ENS, UPMC, UMR 8112 du CNRS, 5 Mail Gay Lussac, 95000 Cergy Pontoise Cedex, France

(Dated: 11 February 2014)

The mobility of O atoms at very low temperatures is not generally taken into account, despite O diffusion would add to a series of processes leading to the observed rich molecular diversity in space. We present a study of the mobility and reactivity of O atoms on an amorphous silicate surface. Our results are in the form of RAIRS and temperature-programmed desorption spectra of O_2 and O_3 produced via two pathways: O + O and O_2 + O, investigated in a submonolayer regime and in the range of temperature between 6.5 and 30 K. All the experiments show that ozone is formed efficiently on silicate at any surface temperature between 6.5 and 30 K. The derived upper limit for the activation barriers of O + O and O_2 + O reactions is $\sim$ 150 K/k_b. Ozone formation at low temperatures indicates that fast diffusion of O atoms is at play even at 6.5 K. Through a series of rate equations included in our model, we also address the reaction mechanisms and show that neither the Eley Rideal nor the Hot atom mechanisms alone can explain the experimental values. The rate of diffusion of O atoms, based on modeling results, is much higher than the one generally expected, and the diffusive process proceeds via the Langmuir-Hinshelwood mechanism enhanced by tunnelling. In fact, quantum effects turn out to be a key factor that cannot be neglected in our simulations. Astrophysically, efficient O_3 formation on interstellar dust grains would imply the presence of huge reservoirs of oxygen atoms. Since O_3 is a reservoir of elementary oxygen, and also of OH via its hydrogenation, it could explain the observed concomitance of CO_2 and H_2O in the ices.

PACS numbers: Valid PACS appear here

Keywords: Astrochemistry, Surface reactions, Molecular Synthesis, ISM, Ozone

arXiv:1402.2211v1 [astro-ph.GA] 10 Feb 2014

[a)]Electronic mail: marco.minissale@obspm.fr

I. INTRODUCTION

The chemical processes taking place in interstellar clouds can be considered the origin of the molecular diversity in the Universe. A wealth of infrared, millimeter- and microwave-wavelength observations has provided evidence of rich molecular abundances within interstellar clouds. This observational evidence for the general interstellar medium (ISM), however, cannot be met by the known gas-phase reactions alone. That is why surface reactions are necessarily invoked for the formation of a growing number of molecular species. Atoms and molecules from the gas phase accrete and gather on the cold surfaces of interstellar dust grains, and eventually react after surface diffusion. In fact, some of the most abundant molecules in the Universe (such as H_2, H_2O or CO_2) are formed on dust grains.[1] Particularly, hydrogenation of interstellar ices is known to induce the formation of species in the solid phase and, recently, O-atom additions as well were invoked for processes leading to an even richer molecular diversity.[1] Due to the supposed high abundance and its certain reactivity, oxygen and its chemistry may then play a central role in astrochemistry.

Gas phase molecular oxygen has been detected[2–4] in molecular clouds (ρ Ophiuchi A and OMC-1) and astrochemical models of dark clouds predict that condensed oxygen is likely to be a major component of apolar ices. Nevertheless, the key O_2 molecule remains elusive in the ISM, very probably owing to its short lifetime,[5] and also because it can be easily consumed at the surface of dust grains by the two most abundant atomic species, H and O, forming H_2O and O_3 respectively, as main products. Water is the most abundant species in the solid phase, while solid ozone has not yet been observed in molecular clouds. To date, only a recent work[6] presents spectra compatible with the presence of O_3 towards IC 5146. This apparent lack of ozone could be explained either by a detection bias as the broad silicate absorption band at 10 μm can easily mask the 9.6 μm ozone feature, or by an actual lack of ozone in the ice.

The non-detection of solid ozone in dense molecular clouds is consistent with its short lifetime on the surface of dust grains due to its high reactivity. Mokrane et al[7] and Romanzin et al[8] have shown that O_3 + H is an efficient process under interstellar conditions and should be able to destroy most of the O_3 formed on the ice to produce water. Water formation on the grain surfaces occurs via hydrogenation of three different oxygen species:[9,10] O, O_2, and O_3. All these routes have been extensively studied in laboratory.[11–14]

Water is ubiquitous and its omnipresence is certainly a result of its stability: among the species made of the 2 dominant reactive atoms H and O, water is the most stable molecule. Figure 1

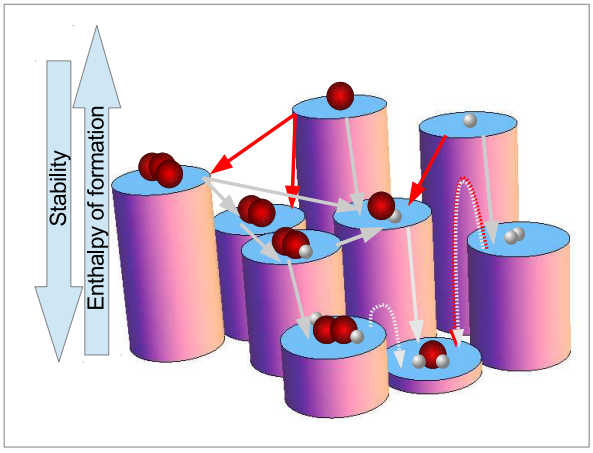

FIG. 1. Schematic 3D representation of the water formation network via H-atom (grey circle) additions to O, O_2, and O_3 (red circles). Enthalpies of reactions grow along the vertical axis. Solid lines represent barrierless reactions, while dotted traces indicate reactions with an activation barrier.

represents all the stable molecules that are composed of O and H atoms. Their enthalpies of formation are represented vertically. We have drawn the different reactions identified experimentally, of which water seems to be the end of the chemical journey in the O and H world. However, to know how hydrogenation of oxygen takes place for forming water, it is necessary to understand how O_2 and O_3 are formed.

In 1930, S. Chapman discovered the mechanisms that produce the ozone layer in the Earth's stratosphere:[15] UV photons striking oxygen molecules (O_2) split them into two oxygen atoms (O); atomic oxygen then combines with O_2 to create ozone. In turn, O_3 can be dissociated by UV light into a molecule of O_2 and an O atom, and so on in a continuing process called the ozone-oxygen cycle, creating an ozone layer in the stratosphere. Recently, ozone formation has been studied in the laboratory using supra thermal oxygen atoms generated by energetic electrons or ions.[16–18] Jing et al[19] also performed experiments on the formation of ozone on bare silicates, but our present work and analysis do not lead to the same conclusions. We attribute the detection of high temperature signals at mass 32 a.m.u. to the decomposition of O_3 inside the quadruple mass spectrometer, and not to the detection of O_2. In this paper we study the surface formation of O_2

and O_3 without the addition of energy, through the reactions:[20]

$$O(^3P) + O(^3P) + M \longrightarrow O_2 + M \quad (1)$$

$$O(^3P) + O_2(X^3\Sigma_g^-) + M \longrightarrow O_3(X^1A_1) + M \quad (2)$$

The substrate, made of amorphous silicate,[21] was held in the 5 – 30 K temperature range. Sub-monolayer conditions were used in all the experiments discussed below. This paper is organized as follows: the experimental set-up and methods are described in the next section. In Section 3, we present our results about O_2 and O_3 formation. In Section 4, we present a model that simulates our results and gives relevant energetic parameters. In the last Section, we discuss the main conclusions and astrophysical implications of this study.

II. EXPERIMENTAL METHODS

Experiments were performed using the FORMOLISM set-up shown in Figure 2, which is described elsewhere[22,23]. The experiments take place in an ultra-high vacuum chamber (base pressure 10^{-10} mbar), containing a non-porous amorphous olivine-type silicate. This sample was obtained by thermal evaporation of San Carlos olivine ($Mg_{1.8}Fe_{0.2}SiO_4$) onto a gold-coated substrate (1 cm in diameter), operating at temperatures between 6.5 K and 350 K. The surface density of adsorption sites is about the same of the one found on compact ice samples.[21] Sample preparation and surface analysis are described extensively in Djouadi et al. 2005.[24] The temperature of the sample T_s is computer-controlled by a calibrated silicon-diode and a thermocouple (AuFe/Chrome K-type) clamped on the sample holder. Via a triply differentially pumped beam, O atoms (and O_2 molecules) are aimed at the cold (6.5-25K) sample. The products are probed using temperature-programmed desorption (TPD) and Reflexion Absorption Infrared Spectroscopy (RAIRS). The TPDs are performed by increasing the surface temperature at 10 K/min. All mass signals are expressed in atomic mass units (a.m.u.).

A. Oxygen beam

Oxygen atoms are obtained by dissociating O_2 gas in a microwave discharge. The dissociation fraction τ can be tuned between 45% and 80% by varying the microwave power. This allows us

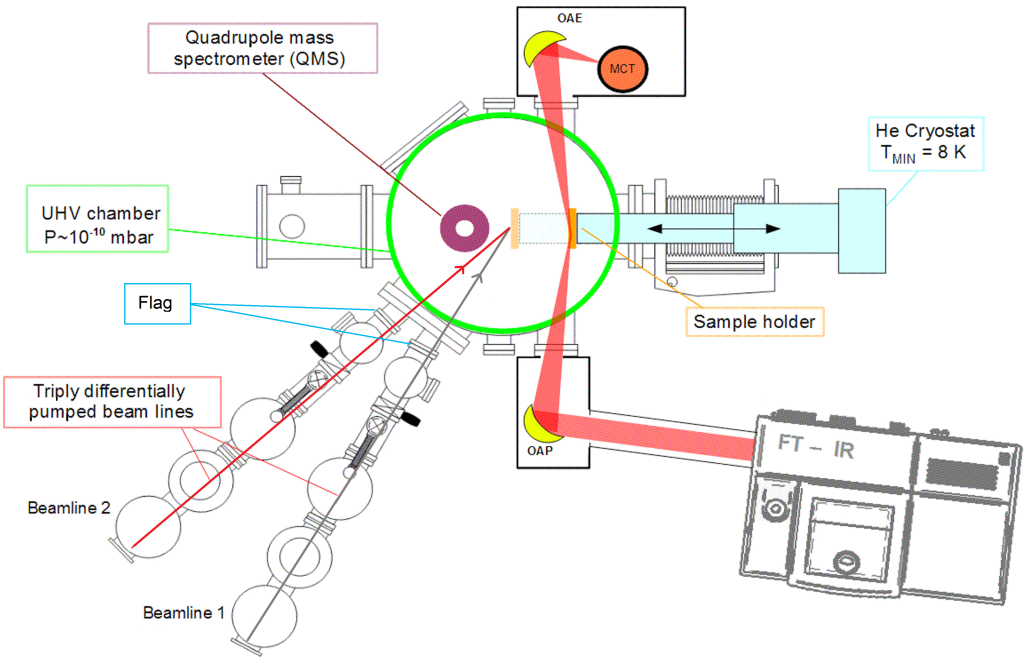

FIG. 2. Schematic top-view of the FORMOLISM set-up and the FT-RAIRS facility.

to change the O/O_2 ratio sent onto the cold sample. 70% of dissociation (typical values used here) corresponds to a deposition with a O_2/O ratio of 3/14 (14 O atoms are produced by the dissociation of 7 molecules). It has been checked that no O_3 was present in the beam. This control was carried out by two different methods. The first control was performed by placing the quadrupole mass spectrometer (QMS) in front of the beam and by monitoring mass-48 signal of the direct beam, and the one of the beam when blocked by a metallic flag. The flag is a metal plate used to intercept the beams before they enter the main vacuum chamber, see Fig.2. The signal at mass 48 was always under the detection limit imposed by electronic noise, and this is a first indication that no O_3 was present in the beam. A second check consisted of irradiating with $O+O_2$ the surface held at 55 K, then performing a TPD. At this temperature the residence time of O and O_2 is extremely short and prevents the formation of O_3 through the reaction $O+O_2$, while gas phase O_3 sticks and remains on the surface. A peak at mass 48 (and mass 32, see below) in the TPD would indicate that O_3 was actually present in the beam. With this second control experiment we could accurately determine that no ozone was present in the O beam.

Also the energetic state of atoms and molecules was checked before commencing the experiments. Molecular orbital theory predicts that the O_2 molecule has two low-lying excited singlet

states, $O_2(a^1\Delta_g)$ and $O_2(b^1\Sigma_g^+)$, while the ground state is the triplet $O_2(X^3\Sigma_g^-)$ state. The energy difference between the lowest energy of O_2 in the singlet state, and the lowest energy in the triplet state is about 11340 K/k_b (T_e ($a^1\Delta_g$ - $X^3\Sigma_g^-$)= 94.3 kJ/mol, 0.98 eV).[25] The required energy to ionize an O_2 molecule in the ground state is 12.07 eV.[26] This means that electrons less energetic than this value cannot ionize O_2 in the ground state, while electrons can ionize $O_2(a^1\Delta_g)$ molecules if they are in the energy range 12.07-11.09 eV. The same argument can be applied for atomic oxygen. O atoms in the ground state (^{3}P) are ionized by 13.6-eV electrons,[27] while in the first excited state ^{1}D the minimum energy necessary for ionization is 11.7 eV (-1.9 eV). Hence, electrons less energetic than 13.6 eV can ionize excited O atoms only. By tuning the energy of the ionizing electrons of the QMS, we can selectively detect ground state or excited state O_2 and O, as described in Congiu et al.[28] Finally, we determined that the beam did not contain O or O_2 in an excited state, nor O_3 molecules. The O beam was thus composed of at least 99% ground-state O and O_2. We also recorded the mass 16 signal in all experiments, and did not detect any signal that could be interpreted as O-atom release in the gas phase. Actually, except for the direct beam, or for a very small fraction (< 2%) due to cracking of O_2 and O_3 in the QMS, we never detected any signal at mass 16. This indicates that O atoms react and never desorb as such, but exclusively as O_2 and O_3 molecules.

B. Determination of O_2 monolayer and flux

The technique used to determine the O_2 flux was adapted from Kimmel et al 2001.[30] The O_2 flux was calibrated by saturation of the first O_2 monolayer[21,29] as shown in Fig. 3. The method consists of depositing different amounts of O_2 – under identical conditions of flux – on the surface maintained at the same temperature (in this case T_s= 10 K). With the increase in the doses deposited on the surface, the TPD curves gradually broaden towards lower temperatures. In fact, as the surface coverage increases, the molecules are adsorbed in less tightly bound adsorption sites, namely the desorption temperature $T_{des} \propto$ desorption energy E_{des} (with peaks growing in height too). When the leading edge of the TPD curves (the left side of the curves shown in the inset of Fig. 3) stops shifting towards lower temperatures, it means that all the adsorption sites on the surface are occupied, and any other incoming molecule is adsorbed on top of the first layer of molecules already adsorbed on the surface. This is when TPDs exhibit a 0^{th} order desorption, the maxima of the desorption peaks increase and start shifting towards higher temperatures with

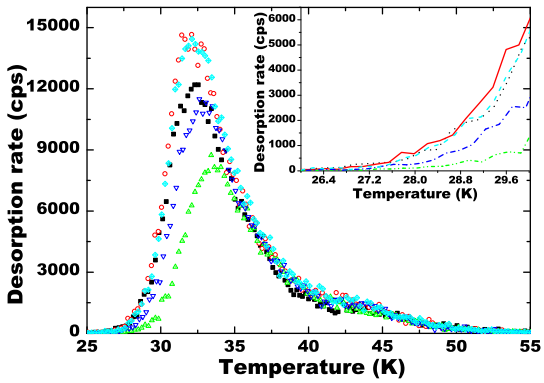

FIG. 3. TPD mass spectra at mass 32 after 240, 270, 300, 330, and 360 s of O_2 exposure on silicate held at 10 K. The inset shows a magnified view of the leading edges between 26 and 30 K.

increasing doses. The unit of coverage we adopt – the monolayer (ML) – is defined as a single layer of atoms or molecules adsorbed on a surface. Here the monolayer coverage of O_2 molecules adsorbed on silicate occurs after 315±30 seconds of O-beam exposure. The integrated signal (expressed in counts per second) over the temperature of the TPD curve after a 315-second exposure corresponds to 1 ML. The same dose is necessary to fill the monolayer if the substrate is made of compact amorphous water, which means that the monolayer is achieved with the same number of molecules (i.e., a similar wetting of the two surfaces occurs). This is not the case (about half of the above dose is needed) if a substrate of graphite is used. Due to the similarity between the behaviours of the silicate and water ice substrates (which implies that the density of adsorption sites is of the same order of magnitude), we can estimate that 1 ML on the silicate sample is 10^{15} molecules cm^{-2}, within the uncertainty of this technique (about 15%). In this work, the doses are expressed in terms of O_2 units, which means that 1 ML may also represent 2 layers of O atoms or 0.66 layers of pure ozone.

C. O_3 detection efficiency and calibration

When using a beam of O_2, it is easy to calibrate the flux and understand when the saturation of one ML occurs. This is not the case for a deposition of O_3. To calibrate one ML of O_3, it is necessary to study and evaluate the cracking pattern and the detection efficiency of ozone by the QMS, with respect to the well known O_2 detection. As already seen in Mokrane et al 2009,[7] the

ozone signal is simultaneously detected at mass 48 and at mass 32 (O_2^+ fragments). This is because the dissociation of O_3 is energetically more favorable than its ionisation (3.77 eV vs 12.53 eV). When O_3 enters the QMS head, it can undergo different processes:

- O_3 (+ e^-) $\longrightarrow$ O_3^+ (ΔH_f = 12.97 eV)
- O_3 (+ e^-) $\longrightarrow$ O_2^+ + O (ΔH_f = 13.17 eV)
- O_3 (+ e^-) $\longrightarrow$ O^+ + O_2 (ΔH_f = 14.72 eV).

The left panel of Fig. 4 shows the TPD spectra at mass 32 and 48 between 55 K and 90 K after a deposition of 5 minutes of oxygen atoms on silicate. The two traces exhibit the same shape, namely, the mass32/mass48 ratio remains constant (right panel of Fig. 4). The two curves are clearly due to the desorption of the same parent molecule (ozone) formed on the substrate. The assignment of the high-temperature peak at mass 32 is the main experimental difference between the interpretation of the data in this work and in Jing et al 2012's.[19] They attribute the O_2 peak desorption between 55 and 90 K to O recombination and subsequence desorption of molecular oxygen. In the present study, we determined that the mass-32 peak is due to ozone desorption and its fragmentation upon detection. The deposition of ozone from ex-situ synthesis confirms this fact: the amount of desorbing ozone can be monitored either via mass 32 or mass 48. By computing the ratio between the two signals (mass32/mass48) after deposition of different doses, as shown in Fig. 4 (right panel), a mean value of 1.5 was found. This fact led us to monitor ozone by the signal at mass 32, instead of that at mass 48, to have a better signal-to-noise ratio.

Due to its important dissociative ionization, ozone detection efficiency has to be determined for every single QMS. Actually, the results that gave the idea of the present work were obtained during two periods of experiments, when two different QMSs were used. Even thought the settings of the two instruments were, at any time, exactly the same, the O_3/O_2 detection efficiencies found were different up to a factor of 30%. For the sake of consistency, however, all the experimental values presented here were obtained with a constant O_3/O_2 detection efficiency. It should also be noted that, for this specific molecule (O_3), any other correction factor among those present in the literature would have be wrong in our case. To estimate the O_3/O_2 detection efficiency at mass 32, it is necessary to compare the area under the TPD curve of one ML of O_2 and that of one monolayer of O_3. Therefore, we also needed to determine for what O-exposure time we reached a complete monolayer of ozone.

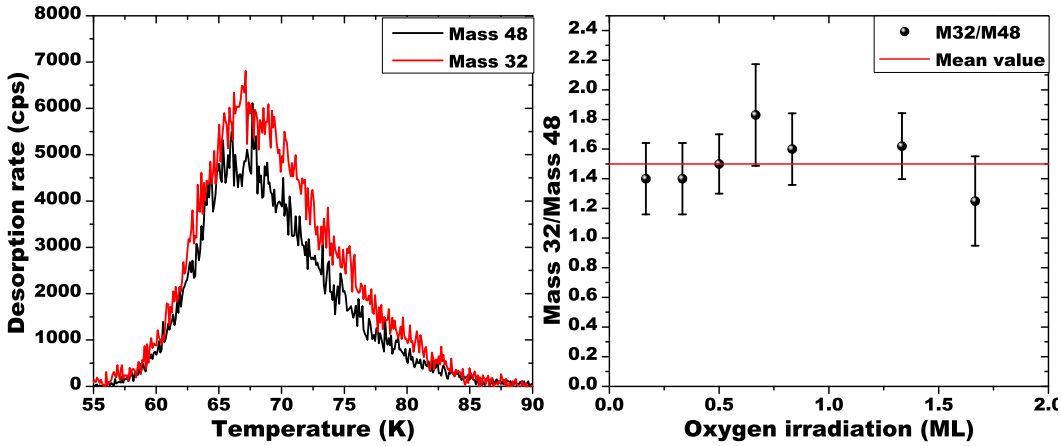

FIG. 4. *Left panel:* Ozone TPD curves at mass 32 and 48 between 55 and 90 K after deposition of 5 minutes of oxygen atoms on silicate held at 10 K. *Right panel:* Ratio of the integrated area of mass 32 and mass 48 TPD peaks (55-90 K) as a function of different doses of oxygen atoms.

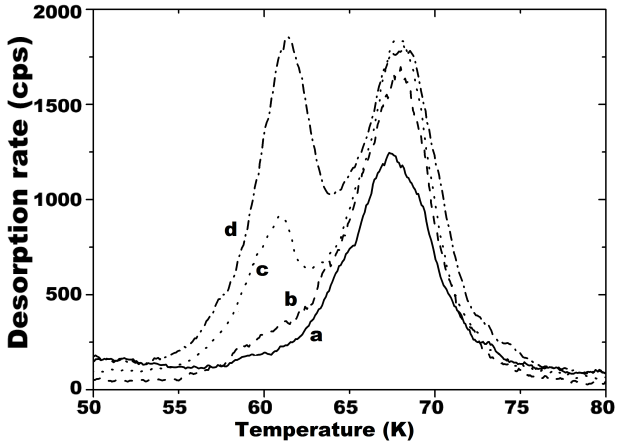

FIG. 5. Ozone TPD curves between 50 and 90 K after four depositions of oxygen atoms of (from *a* to *d*) 6, 8, 10, and 12 minutes on silicate held at 10 K. Curve *b* represents desorption of a complete ozone monolayer, while *c* and *d* exhibit also another peak at ~60 K due to desorption of O_3 from the second layer.

To calibrate the ozone monolayer, we adopted the same first layer-saturation method used for O_2. To do so, we gradually increased the amount of ozone formed on the surface (via $O+O_2$ reaction), until the second-layer desorption peak appeared. In fact, the second-layer desorption peak is a clear signature that the first monolayer has been completed and that a new layer is being grown. In Fig. 5, we show four TPD curves of ozone obtained by increasing the exposure time of oxygen atoms (from curve *a* to *d*). The saturation of the first layer corresponds to trace *b*, and

the appearance of the second peak is observed in trace c. The apparent inconsistency between the TPD peak intensity in Fig. 4 (left panel) and Fig. 5 is due to different QMS settings. Nevertheless, we cannot be certain that the adsorption site density for ozone is the same seen for molecular oxygen. Also, by applying the derived efficiency detection factor (ef), we found that the number of O atoms desorbed as O_2 and O_3 were fewer than the number of O atoms exposed. This may seem non-consistent with the results found in a previous study on water ice.[31] We demonstrated, however, that the missing atoms in the case of the silicate substrate, are due to the prompt release of molecules upon formation, the so-called chemical desorption.[32] Therefore, the amorphous silicate substrate is not suitable for calibration measurements.

When working on a water ice substrate instead, the surface-saturation method gives a reliable detection efficiency and an exact linear relation between the products and the deposited species. For this reason, the water ice substrate assures that the efficiency factor ef is correctly estimated. Moreover, the density of adsorption sites for O_2 and O_3 is identical. We then expect that the total number of O atoms and O_2 molecules sent onto the water ice substrate is conserved and it is equal to $O+O_2+ef\times O_3$. To check the conservation of O atoms, all the species are normalized to the O_2 signal (the O signal is divided by 2 and that of O_3 is multiplied by 1.5). Different doses of $O+O_2$ are then sent onto the icy substrate and a typical set of temperature-programmed experiments is performed.

The dashed line in Fig. 6 corresponds to TPD yields after pure O_2 deposition carried out with the undissociated beam. The red squares in Fig. 6 were obtained through integration of the area under the O_2 TPD curves of mass 32 between 25-50 K. The blue stars correspond to the integration of the ozone signal multiplied by the efficiency factor. The green triangles are obtained by adding the O_2 and the corrected O_3 ($ef\times O_3$) contributions. These contributions lie – within the experimental errors – on the line given by the total amount of deposited O atoms, which indicates that both the efficiency factor used and the monolayer calibration are reliable. It must also be noted that the O_3/O_2 ratio varies greatly with the coverage, so if the efficiency factor is not correctly estimated, the total O_2 + O_3 yield cannot be proportional to the initial dose. To show the reliability of our ef factor, in Fig. 6 we drew a shaded area indicating a $\pm 30\%$ variation of ef. Finally, the two independent estimations of the monolayer coverage and the fact that the number of O atoms is conserved, regardless of the ratio of O and O_2 sent onto the surface (and the O_2 and O_3 ratio desorbing from the surface), clearly suggests that our calibrations were correct.

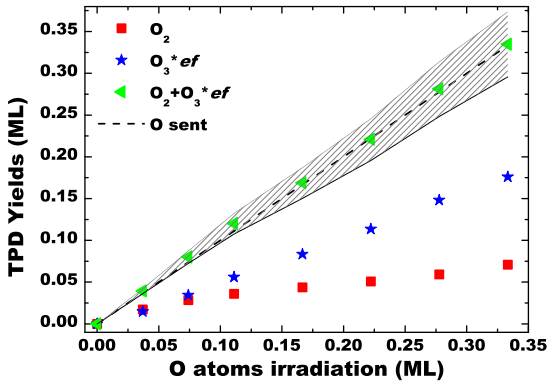

FIG. 6. Integrated areas (in ML) of the TPD peaks of O_2 (red squares) and O_3**ef* (blue stars) vs O-atom fluence. Green triangles: sum of O_2 and O_3**ef*. The dashed line represents the total amount of oxygen atoms deposited on the surface. The shaded region indicates a ± 30% variation of the efficiency factor *ef*.

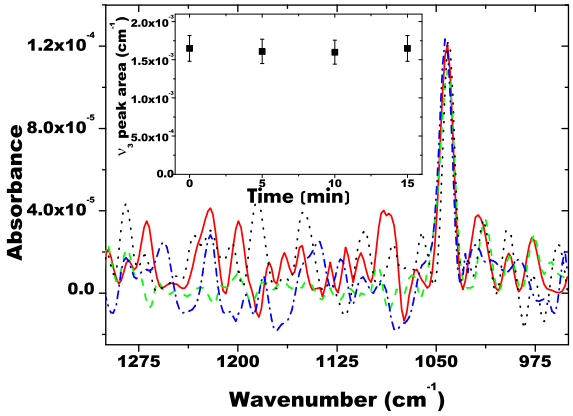

FIG. 7. Series of RAIR spectra recorded at different times after deposition of 0.3 ML of O atoms at 6.5 K; the absorption bands at 1043 cm^{-1} is because of the ν_3 asymmetric stretching mode of O_3. Inset: ν_3 band integrated area as a function of wait time (0, 5, 10, and 15 min).

III. EXPERIMENTAL RESULTS

All the experiments described below indicate that ozone is formed efficiently on silicate at any deposition temperature of the surface between 6 and 25 K. The first evidence of ozone formation is in the infrared spectrum recorded after depositing 0.3 ML of atomic oxygen on silicate held at 6.5 K (Fig. 7). 0.3 ML also represents the lower detection limit of the ozone band in our IR spectrometer. Working with low coverages is the key to understanding what mechanism is at play

in ozone formation. There are mainly two mechanisms that may lead to ozone. The Eley-Rideal mechanism (ER) occurs when one of the molecules already adsorbed promptly reacts with a particle coming from the gas phase, before being adsorbed on the surface. The Langmuir-Hinshelwood mechanism (LH) describes the formation of molecules on a surface when two adsorbed reaction partners react because of the diffusion of at least one of them. ER is independent of T_s, and it becomes more efficient with the increase in surface coverage. At high coverages (more than one ML) it becomes the most probable mechanism. Conversely, the LH mechanism is initiated by the mobility of the species and is very sensitive to T_s. Whenever the diffusion is fast enough, it may be efficient also at low coverages (see below). In Fig. 7, we show the ν_3 asymmetric stretching mode of $^{16}O_3$ at 1043 cm^{-1}.[33,34] The weak bands at 1103 and 700.9 cm^{-1} are not visible due to our experimental conditions. The presence of the ν_3 band indicates that ozone was formed already at 6.5 K. Moreover, this band does not evolve with time (simply by waiting 5, 10, or 15 minutes at 6.5 K), as shown in the inset of Fig. 7, where the squares represent the integrated area under the peaks. In the left panel of Fig. 8 we show how the ozone band evolves with temperature. The squares in Fig. 8 (right panel) represent the total absorbance by integration of the O_3 band as a function of surface temperature. The intensity of the band does not change within the limits of the error bars. This indicates that no ozone was formed during the heating, when the diffusion and reactivity of the ad-atoms (if present) should increase. In fact, the reactions leading to ozone formation had already occurred at the deposition temperature via the LH mechanism. However, due to the size of the error bars, a small increase of the ozone band could have still been possible. We estimated that an upper limit for the fraction of extra ozone formed during the heating is 15%, a value that we will use below in the discussion.

To disentangle the ER from the LH mechanism, one should vary the coverage, since ER is very sensitive to it, and the temperature of the surface since the LH mechanism efficiency is governed by the diffusion at a given temperature. We then deposited equal amounts of $O+O_2$ for a total of 0.3 ML at different T_s, and performed a TPD at 10 K/min after each deposition. The resulting TPD traces are presented in Fig. 9. In each mass spectrum, two desorption peaks appear: O_2 desorbs between 35 K and 50 K, while ozone desorption is observed between 55 K and 75 K (directly at mass 48, or via the O_2^+ fragments at mass 32). O desorption was never observed. The height of the peaks (proportional to the amount of the species formed on the surface) changes depending on the coverage and on the surface temperature. Fig. 9 summarizes the outcome of six TPDs, in which the coverage was fixed (0.29 ± 0.03 ML) and the deposition temperature varied between 8 K and 30

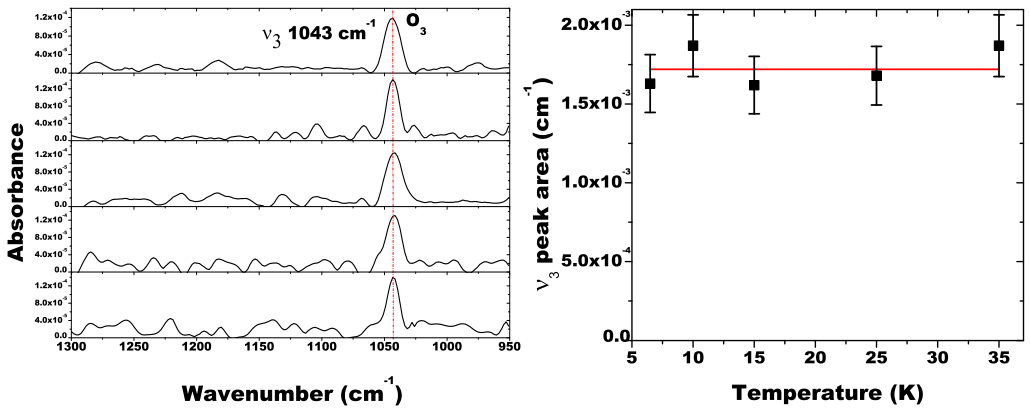

FIG. 8. *Left panel:* RAIR spectrum obtained at different T_s (bottom to top, 6.5, 10, 15, 25 and 35 K) after deposition of 0.3 ML of O atoms at 6.5 K; the absorption band at 1043 cm^{-1} is due to the ν_3 asymmetric stretching mode of O_3. *Right panel:* integrated area of the ozone band as a function of surface temperature. The red solid line represents the mean value of the five integrated band areas.

K. We can observe, from curve to curve, a clear change in the O_3/O_2 ratio. This effect is due to the temperature of the silicate substrate and is a sign of the role of diffusion in the formation of ozone. In fact, with increasing surface temperature, the mobility of O atoms is favored, ozone formation is more efficient, and the O_3/O_2 ratio increases. Each new adsorbed atom – if the diffusion is fast – is able to scan the surface to react with O_2 to form O_3, or with another absorbed O atom to form O_2 (that, in turn, will also be transformed into O_3 by the next incoming and mobile atom). In this scenario, almost all O atoms and O_2 molecules are transformed into O_3 molecules. On the contrary – if the diffusion is slow – an oxygen atom has not enough time to scan the surface and react with an adsorbed O_2. Another O atom then comes and more O_2 is formed via the O+O reaction. A reduced mobility leads to the accumulation of O atoms on the surface, the probability for an O atom to meet another O atom raises, and eventually the O_2 formation is favored.

By comparing RAIRS and TPD results, it is possible to see how the diffusion of O atoms changes the O_3/O_2 ratio. As stated above, we have assumed that an increase of 15% of the ozone yield may have occurred during the heating from 6.5 to 35 K (see Fig. 8). From TPD results, however, we obtain a variation of 47% between the ozone yields after O deposition performed at 8 K and the one performed at 30 K. This indicates that, taking into account the possible 15% contribution due to the heating, there is a 32% (47 from TPD, -15 from RAIRS) difference between TPD experiments carried out at T_s=8 and 30 K. In the upper panel of Fig. 10 we show TPD (blue stars) and RAIRS

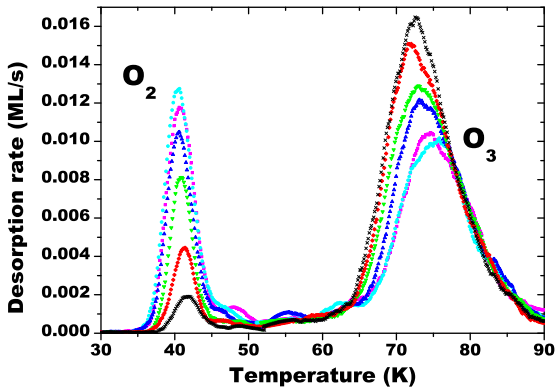

FIG. 9. Series of 6 TPD curves after deposition of 0.3 ML of O atoms on silicate held 8, 10, 15, 20, 25, and 30 K. The low temperature peak (O_2) decreases with deposition temperature while the high temperature peak (O_3) grows bigger with increasing deposition temperatures.

(green shaded region) normalized peak areas (yields) of ozone. TPD variations (also considering the error bars) are greater than the ones in RAIRS data. This difference is clearly an effect due to T_s, i.e., variations of O atom mobility on the silicate surface. In the lower panel of Fig. 10 we show the O_2 yield variations in TPD experiments after O exposures at various T_s, normalized with respect to the TPD yield after deposition of O atoms at 8 K. In depositions carried out at 30 K, only 15% of the amount of O_2 formed at 8 K was observed.

Fig. 11 shows the integrated peak areas of O_2 and O_3 TPDs as a function of the amount of deposited O atoms. Exposures were performed at T_s=10 K with coverages going from 0.1 to 1.0 ML. Red squares represent the molecular oxygen yield and blue stars represent the ozone yield. The O_2 production reaches a value of little less than 0.2 ML, with a growing rate diminishing with the coverage. On the other hand, the ozone yield increases with the coverage and reaches a value of about 0.5 ML. Green triangles in Fig. 11 represent the sum of the ozone and oxygen integrated peak areas while the dashed line is the total amount of oxygen atoms sent onto the surface. The discrepancy between the total yield of products (O_2 + O_3) and the dashed line – indicating a non-conservation of oxygen atoms – is due to the the chemical desorption of oxygen molecules.[32] It is clear, from Fig. 11, that the difference between the number of atoms sent onto the surface and those detected is maximum in the range of coverages between 0.2 and 0.5 ML, i.e., in the low coverage regime where chemical desorption is more effective.

To have a better understanding of the mechanisms occurring on the silicate surface, we have

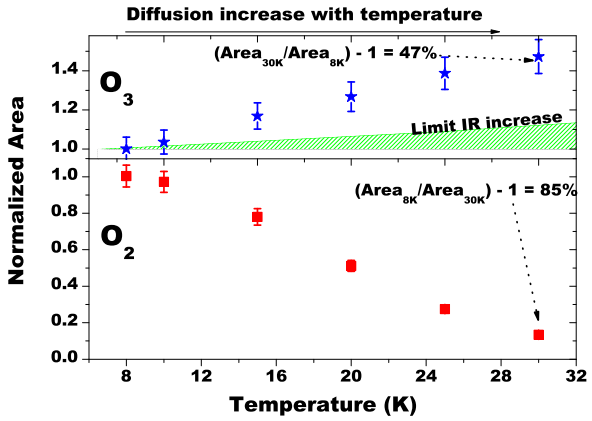

FIG. 10. Integrated peak areas of O_2 (lower panel, red squares) and O_3 (top panel: blue stars) yields (obtained in the experiments shown in Fig. 9) vs deposition temperature. The peak areas were normalized w.r.t. the TPD yields after deposition at 8 K. Green pinstriped region: range of values of the O_3 signal increase due to thermal diffusion derived from IR spectra.

developed a model that we present in the next section. Our model was conceived to fulfill the following experimental evidences:

1. The O_3/O_2 ratio depends both on the coverage and on the surface temperature.

2. At T_s = 6.5 K, with 0.3 ML of O-atom coverage, more than 85% of ozone is formed during the deposition phase.

3. Experimental data confirm that chemical desorption of O_2 molecules occurs, and its efficiency seems to decrease with coverage. To simplify our model, however, we have assumed a constant chemical desorption rate.

IV. MODEL

The O_2 and O_3 formation can occur via the following exothermic reactions:

$$O + O \longrightarrow O_2 \tag{3}$$

$$O + O_2 \longrightarrow O_3 \tag{4}$$

$$O + O_3 \longrightarrow 2O_2 \tag{5}$$

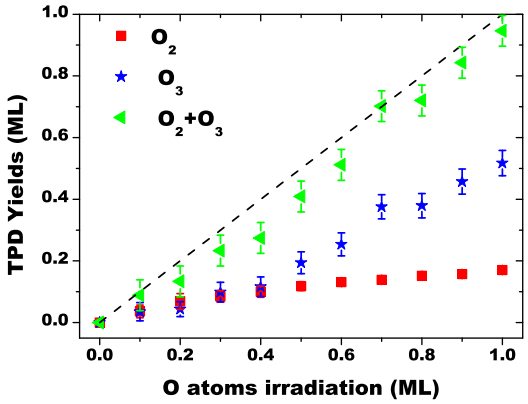

FIG. 11. Integrated peak areas of O_2 (red squares) and O_3 (blue stars) yields as a function of O-atom dose at 10 K. Green triangles: sum of O_2 and O_3 yields. The dashed line represents the total amount of oxygen atoms deposited on the surface.

The exothermicity of these reaction is 5.2 eV, 1.1 eV and 4.0 eV, respectively. If reaction (5) were efficient, it would cause a decrease in the ozone amount and double an increase in molecular oxygen. However, taking into account the fact that the ozone production efficiency is close to unity at high temperature or high coverage, the third reaction is apparently not efficient under our experimental conditions. Hence we can neglect it and assume that this is probably due to a barrier to the O + O_3 reaction. We will include this reaction later in the discussion to estimate the height of the barrier, and check whether our initial assumption is reasonable.

By supposing that the reactions leading to O_2 and O_3 are governed by the density of species on the surface and by T_s, we can model the processes through a series of rate equations. We tried to fit our data by using different approaches, and tested different hypothesis. Our model includes both ER and LH mechanisms. It also allows reactions to occur during the heating ramp, as well as during the exposure phase, even if we know – thanks to the IR spectra – that this contribution should be small. In addition, our model assumes a constant sticking coefficient, namely one for all species. The free parameters of our model are the reaction barriers and the O diffusion efficiency.

Other parameters are the dissociation fraction τ and the chemical desorption rate that have been measured previously. Actually, the chemical desorption could have been neglected in this study, we put it in our model because it increases the quantitative quality of the fitting. The chemical desorption was already studied in Dulieu et al 2013,[32] and in the case of newly formed O_2 on silicate has a value of 40% ± 10%.

The dissociation fraction τ can be easily calculated by using this equation:

$$\tau = \frac{(CPS\,O_2)_{Off} - (CPS\,O_2)_{On}}{(CPS\,O_2)_{Off}} * 100 \tag{6}$$

where $(CPS\,O_2)_x$ indicates the counts per second when the discharge is off or on, with the direct beam passing through the QMS. Typical values of τ are between 45-80%. This is taken into account through the term $(1-\tau)\phi$, where ϕ is the normalized flux of O_2 molecules when the discharge is off. Similarly, the term $2\tau\phi$ represents the flux of oxygen atoms. The rate equations used in our model are:

$$\begin{aligned}\frac{d[O]}{dt} = {} & 2\tau\phi(1 - 2O\,r_1 - O_2\,r_2) - (1-\tau)\phi\,O\,r_2 + \\ & -4k_x\,OO\,r_1 - k_x\,OO_2\,r_2 \\ & -4k_{td}\,OO\,r_1 - k_{td}\,OO_2\,r_2\end{aligned} \tag{7}$$

$$\begin{aligned}\frac{d[O_2]}{dt} = {} & (1-\tau)\phi\,(1 - Or_2) - 2\tau\phi\,(O_2 r_2 - Or_1) + \\ & +2k_x\,OO\,r_1\,(1-\epsilon) - k_x OO_2 r_2 \\ & +2k_{td}\,OO\,r_1\,(1-\epsilon) - k_{td} OO_2 r_2\end{aligned} \tag{8}$$

$$\begin{aligned}\frac{d[O_3]}{dt} = {} & (1-\tau)\phi\,O\,r_2 + 2\tau\phi\,O_2\,r_2 \\ & +k_x\,OO_2\,r_2 \\ & +k_{td}\,OO_2\,r_2\end{aligned} \tag{9}$$

where O, O_2, and O_3 are the surface densities (expressed in fraction of ML) of each species, ϕ is the flux (0.003 cm^{-2} s^{-1}) of O_2, ϵ is the evaporation probability due to the chemical desorption, k_x is the diffusion probability expressed in ML^{-1} s^{-1} (which can be converted into the usual unit cm^2 s^{-1} by considering that 1 ML = 10^{15} molecules cm^{-2}), and

$$r_1 = \nu e^{-\frac{E_{OO}}{k_b T}} \tag{10}$$

$$r_2 = \nu e^{-\frac{E_{OO_2}}{k_b T}} \tag{11}$$

$$k_{td} = \nu e^{-\frac{E_d}{k_b T}} \tag{12}$$

are the O+O and O+O_2 reaction probabilities, and thermal diffusion probability during the heating, respectively. E_{OO} and E_{OO_2} are the barriers of reactions (3) and (4), E_d is the diffusion barrier (all barriers are expressed in K/k_b) and ν=10^{12} s^{-1} is the trial frequency for attempting a new event. The

diffusion rate k_x (at a fixed T_s) includes two components due to quantum tunneling and thermal motion:[31]

$$k_x = k_{qt} + k_{tm} \tag{13}$$

In practice, the diffusion rate during the deposition phase is governed by a free numerical parameter, whereas the diffusion coefficient during the heating ramp (k_{td}) is described by a classical thermal hopping mechanism (Arrhenius-type law). It is possible to use a free parameter during the exposure because the coverage evolution is known and this represents a strong constraint, and because the diffusion is supposed to be constant at constant temperature. However, if the diffusion during the deposition phase followed an Arrhenius behavior, it would be possible to recognize it a posteriori. We decided to use the Arrhenius law during the heating ramp, as most authors did, to compensate for the absence of constraints on the coverage (O, O_2 and O_3 populations are not known at the beginning of desorption) and to describe the evolution of the diffusion with temperature.

In the rate equations (7), (8), and (9) the ER mechanism is represented by the terms including the beam flux ϕ. On the other hand, the LH mechanism appears in the terms that include the diffusion occurring during the deposition phase, k_x, or during the heating phase, k_{td}. By using this model, we can test, either each at a time or both at once, the two mechanisms to see how they affect the experimental observables.

A. Model 1: ER and thermal diffusion during TPD with barrieless reactions.

In the first model, we suppose that reactions occur only through the ER mechanism (during deposition) or later during the heating phase (TPD). We assume that there is no diffusion of atoms at low temperature (k_x=0). This is an extreme assumption where the diffusion cannot occur during the exposure, and especially any tunneling effect is discarded at the lowest temperatures. We have also assumed that all reactions are barrierless (except for the $O+O_3$ reaction).

In Fig. 12α and β we show two results of this model (solid lines) and compare them to the experimental values. The left panel (α) represents the O_2 and O_3 yield evolution with coverage and the right panel (β) shows the evolution with temperature. In these models, we have tested diverse values of the diffusion efficiency during the TPD, namely, between E_d=100 K/k_b (i.e., a very fast diffusion), and E_d=900 K/k_b (i.e., slow diffusion). From model 1, we conclude that it is not pos-

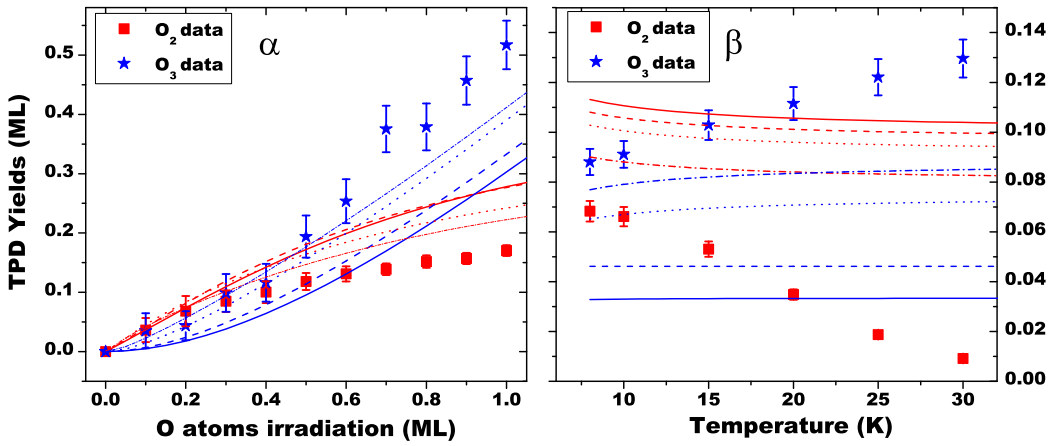

FIG. 12. Left panel (α): TPD yields vs coverage, comparison between model 1 and experimental data. Right panel (β): TPD yields vs surface temperature. Model details: diffusion barrier = 100 K/k$_b$ (solid line), 300 K/k$_b$ (dashed line), 550 K/k$_b$ (dotted line), 900 K/k$_b$ (dashed-dotted line).

sible to fit our data assuming barrierless reactions and without considering diffusion during the deposition phase.

B. Model 2: ER+LH+thermal diffusion with reaction barriers as free parameters.

Here we include the possibility of diffusion during the exposure phase and we allow the two reaction barriers (E$_{OO}$ and E$_{OO_2}$) to vary freely in the range 100 – 900 K/k$_b$. We then analyzed the results by applying a minimization method between model and data for each case. The results are shown in Fig. 13α and β. We can see that a reasonable match was found, although no E$_d$ value satisfies both coverage and T dependencies at once. In fact, the low diffusion case (E$_d$=100 K/k$_b$) gives the best fit as far as the temperature evolution is concerned (Fig. 13β), but gives the worst fit for the coverage evolution (Fig. 13α), whereas the high diffusion case (E$_d$=900 K/k$_b$) gives the best fit with coverage (Fig. 13α) and the worst fit with temperature (Fig. 13β). As suggested by the infrared spectra of O_3 at 6.5 K, the diffusion of atoms during deposition is a key element of the present study. Hence, it was important to test if the model was able to reproduce the experimental results obtained during the deposition phase. We found that experimental values cannot be met if we neglect the diffusive processes. Moreover, we also demonstrated that we could have obtained opposite conclusions if we had used only the temperature, or only the coverage evolutions of the

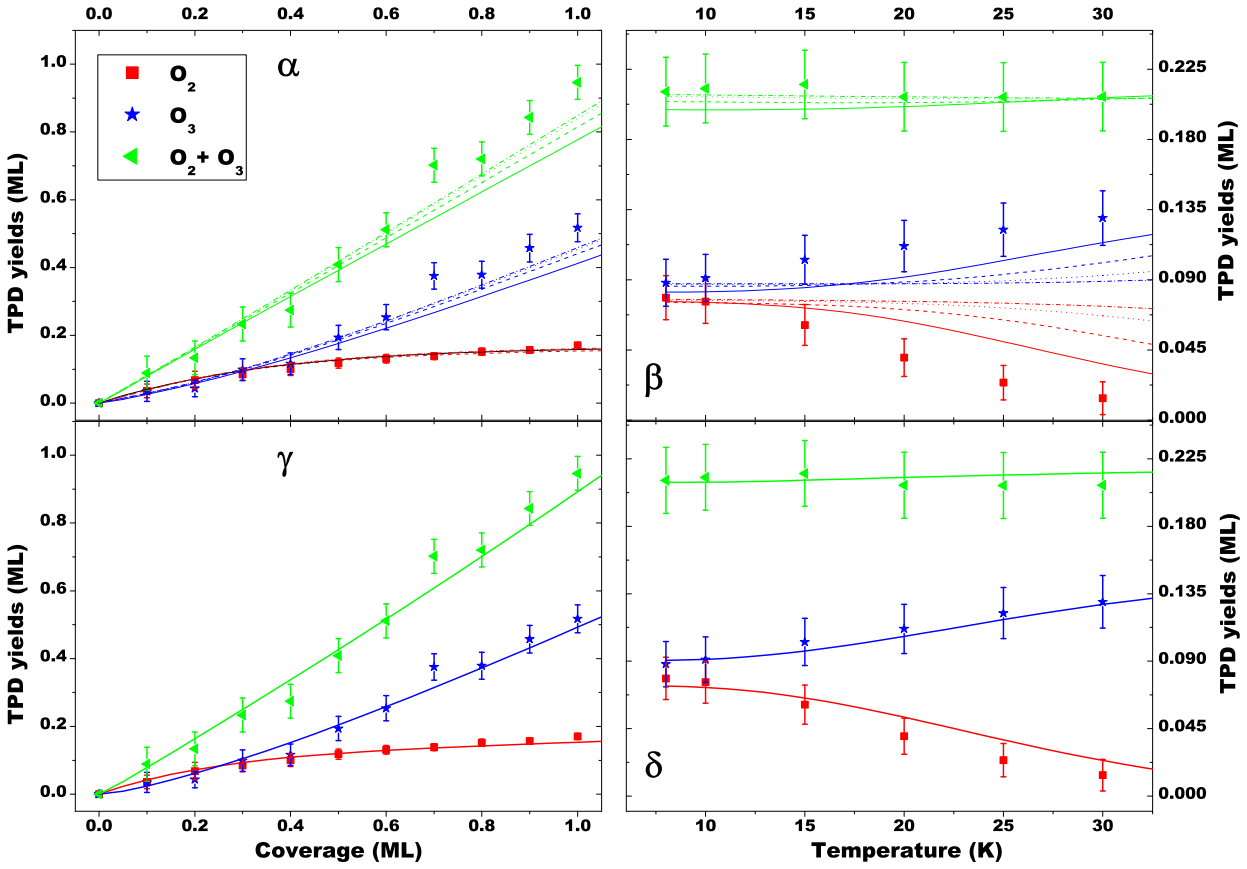

FIG. 13. Comparison between model 2 and experimental data (α and β panels). *Case* α: TPD yields vs coverage, *Case* β: TPD yields vs surface temperature (T_s). Activation barriers in α and β: 100 K/k_b (solid line), 300 K/k_b (dashed line), 550 K/k_b (dotted line), 900 K/k_b (dashed-dotted line). Comparison between model 3 and experimental data (γ and δ panels). *Case* γ: TPD yields vs coverage,, *Case* δ: TPD yields vs surface temperature. Diffusion rates $k_x(T_s)$ are given in Table 1.

O_2 and O_3 yields.

C. Model 3: ER+LH+thermal diffusion with barrierless reactions.

In this model we simulate the same processes seen in the previous section, but using barrierless reactions (except for the $O+O_3$ reaction). The model results displayed in Fig. 13γ and δ show a very accurate fit of our data. It is important to point out two aspects of these results. First, when $0<E_{OO}=E_{OO_2} < 150$ K/ k_b, we find several minima in the χ^2 and we cannot choose a precise value for E_{OO} and E_{OO_2}. Actually, if we assume that there is no barrier to the reactions, the results are

TABLE I. Diffusion coefficients as a function of surface temperature.

$\mathbf{T_s(K)}$ / $\mathbf{k_x}$	8	10	15	20	25	30
$\mathbf{ML^{-1}\ s^{-1}}$	0.10	0.13	0.25	0.5	1.1	2.6
$\mathbf{cm^2\ s^{-1}\times 10^{-16}}$	1	1.3	2.5	5	11	26

almost identical. From our simulation we conclude that the activation barriers are so low that they do not slow down reactions (3) and (4) occurring on the surface. We can only derive an upper limit for the two barriers of about 150 K/k_b. It is therefore possible to set the reaction probability equal to one (barrier equal to zero), and the model remains still fully satisfactory. In Table 1 we show a series of diffusion parameters we obtained using barrierless reactions. The diffusion of atoms increases with the temperature, and follows a T^n law, with n=3 giving the best fit. On the contrary, using an Arrhenius-type law, this is not possible, or, if we try, the best fit parameters do not have a plausible physical meaning (i.e., a very low energy and a very low trial frequency). For this reason, we believe that, on amorphous silicate, as occurs in the case of water ice,[31] quantum tunneling should be an important mechanism at low temperature, although we observe a slower diffusion on amorphous silicate than on water ice.

The second important point is that during the heating phase the diffusion is almost negligible. In fact, not more than a few % of the O atoms deposited are still present on the surface in the very low coverage and temperature regime. For this reason, the effect of a possible diffusion during the TPD lies within the error bars of the experimental data. This also validates our assumptions based on IR spectra recorded at 6 K.

In conclusion, the simplest and most efficient description of our TPD data is to consider a system that is limited only by the diffusion during the exposure phase (LH-dominated), and only slightly adjusted by adding the ER mechanism, especially in regimes of high coverage ($\geq$ 1 ML).

D. Evaluation of $O+O_3$ activation barrier

Here, we want to test whether the reaction $O+O_3$ takes place or not. In our model, we then added the following terms to the right side of Eq. (7), (8), and (9), respectively:

$$-2\mu\phi O_3 r_3 - k_{td} O O_3 r_3 - k_x O O_3 r_3$$
$$2(\mu\phi O_3 r_3 + k_{td} O O_3 r_3 + k_x O O_3 r_3)$$
$$-2\mu\phi O_3 r_3 - k_{td} O O_3 r_3 - k_x O O_3 r_3$$

where

$$r_3 = \nu e^{-\frac{E_{OO_3}}{k_b T}} \tag{14}$$

is the $O+O_3$ reaction probability and E_{OO_3} is the barrier to reaction (5). By varying E_{OO_3}, we noticed that even for values bigger than ~ 2000 K/k$_b$, the amount of O_2 and O_3 remained unaltered; while for values of $E_{OO_3} < 2000 K/k_b$ the χ^2 started to increase. To give an estimate of a lower limit of the barrier, we took the error bars as the borders limiting a the maximum allowed amount of O_2 yield (the smaller E_{OO_3} the more O_2 is produced). We found a reaction barrier of 2300 K/k$_b$. This means that the barrier is very likely to be greater than this value. In addition, this value is consistent with the data available in gas phase, where barriers were found to be greater than 1950 K/k$_b$.[35] This convincingly shows that the $O+O_3$ reaction is slow enough that it can be neglected in our model.

E. Hot Atom mechanism

Generally, only ER and LH mechanisms are considered when the formation of molecules via surface chemistry is concerned. However, a molecule arriving at the surface may not be chemisorbed (or physisorbed) upon the first impact due to the inefficient energy transfer between the impinging particle and the surface. Before the complete dissipation of its incident energy, the adsorbed particle is not in thermal equilibrium with the surface. Hence, impinging particles could be able to hop on the surface and react with already adsorbed molecules lying several angstroms away from the impact site. In the literature, this process is called "Hot Atom" (HA) or Harris-Kasemo[36] mechanism. To date, HA has been studied mainly from a theoretical point of view (Martinazzo et al 2004,[37] and Molinari & Tomellini 2002,[38] and ref. therein), although some experimental studies exist (Wei & Haller 1996,[39] and Dinger et al 2001,[40] and ref. therein). Previous works considered metallic surfaces only, and atoms with an energy greater than 0.5 eV or light atoms (H or D); under these conditions, the energy transfer between the particles and the surface

is slow, so there is a high probability that the HA mechanism occurs. In our experiments, we worked under very different conditions. We performed the experiments on non-metallic surfaces (silicate, graphite, and water ice), atoms had an energy < 0.01 eV and were heavy particles (O atoms, mass(O)/mass(H)=16). These considerations lead us to assume that the HA mechanism should not be important under our experimental conditions, especially at low coverages. Another problem – still unsolved to date – is the surface temperature dependence of the HA mechanism. Some experimental and theoretical works (Quintas-Sánchez et al 2013,[41] and ref. therein) show a temperature dependence of HA, but the range of temperature used is very broad (more than 300 K). In our case, the range of the surface temperatures is small (< 25 K) and it is reasonable to assume that the energy transfer between an adsorbed particle and the surface is quite constant within this range of temperatures. We tried to include the HA mechanism in our model taking into account all the points discussed above. It turns out that the HA mechanism does not exhibit a surface temperature dependence under our experimental conditions, and we may consider it as an "enhanced ER mechanism": atoms coming from the gas phase are likely to scan more than one adsorption site and thus have a higher probability to react. In Fig. 14, we show the results of the model for O_2 and O_3 yields vs coverage (left panel) and O_2 and O_3 yields vs surface temperature (right panel). The curves shown in the figure were generated by considering 5 cases: HA does not take place (0 jumps, solid line) or HA takes place and the atoms are able to scan 3, 5, 8 or 10 sites. The traces displayed in the left panel (3-5 jumps) seem to fit the experimental data although this is not the case for the curves in the right panel, where the temperature independence of ER and HA prevents the model from converging to a good fit for O_2 and O_3. In this case, the temperature dependence is contained only in the Arrhenius term used to simulate the TPD. Regardless of the diffusion barrier we may use (in the case shown in Fig. 14, E_d is 500 K/k_b), we are not able to reproduce the plateau behavior of the experimental values. In fact, the exponential law induces a sudden change (shifted towards low or high temperature depending on the value of E_d) in the yields O_2 and O_3.

The lack of theoretical and experimental studies about HA under the same conditions used in the present work (a non-metallic surface, low energy and heavy atoms), together with the results of our model, suggests that HA cannot explain the experimental results. This corroborates the hypothesis that the diffusion mechanism (LH) is dominant at low temperatures and in low coverage regimes.

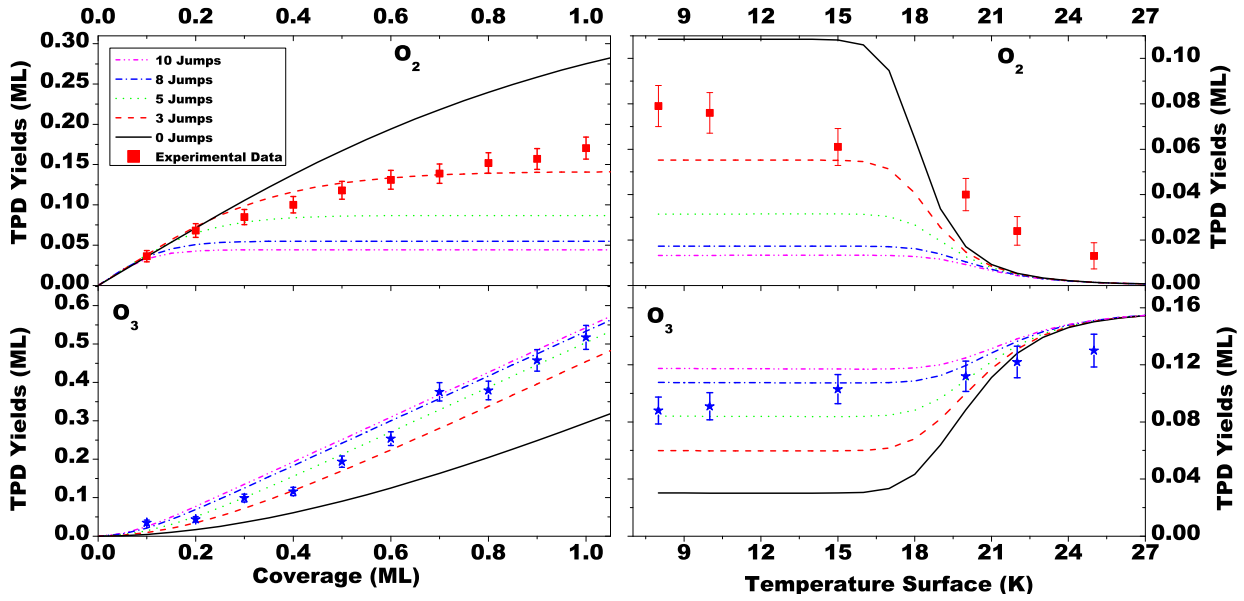

FIG. 14. Comparison between model 2 + Hot Atom mechanism and experimental data. *Left panel*: O_2 (top) and O_3 (bottom) TPD yields vs coverage. *Right panel*: O_2 (top) and O_3 (bottom) TPD yields vs surface temperature. Model results (lines) are generated by considering 5 cases: HA does not take place (0 jumps, solid line) or HA occurs and the atoms are able to scan 3, 5, 8 or 10 adsorption sites (dash, dot, dash-dot and dot-dash-dot curves, respectively).

V. CONCLUSIONS AND ASTROPHYSICAL IMPLICATIONS

In this paper we have shown that O_3 can be formed very efficiently via an atomic oxygen beam sent on silicate held at low temperatures (6-30 K). The reactions leading to ozone formation studied in this paper (O+O and O+O_2) appear to be barrierless; we have estimated an upper limit for the activation energies of reactions of 150 K/k_b. Conversely, the reaction O+O_3 has a high activation barrier – lower limit $\sim$ 2300 K/k_b – and it is not an efficient pathway for ozone destruction under our experimental conditions. In addition, the formation of ozone is favored by a very fast diffusion of oxygen atoms at low temperatures. The diffusive process of O atoms is likely to occur via quantum tunneling, as claimed in Minissale et al 2013,[31] while the Hot Atom mechanism effects proved to be negligible.

From an astrophysical point of view, since the gas phase abundances of O and O_2 are elusive,[42,43] it is difficult to put the O_3 formation in a simple interstellar contest. New and more detailed observational data are necessary to know the solid phase abundances of ozone. Anyway, we can fairly assume that in dense clouds, particularly UV-protected interstellar environments ($A_v > 3$),

if comparable budgets of O atoms and H atoms are present,[44] an O-addition chemistry competes with H additions and O_3 could be formed. The presence of ozone in the interstellar ices would confirm that the O_3+H pathway is the most important route leading to water in some interstellar environments. Not only ozone is important because it represents an efficient way to produce water, but also because it can be a reservoir of oxygen atoms; due to its low binding energy (1.1 eV), ozone can be easily processed by cosmic-rays and by the mean Galactic UV field,[10,45] producing O atoms that, for example, could react on the surface of dust grains with CO and produce CO_2.[46,47] Even without energetic events, CO+OH[48,49] and CO+O[50] reactions are believed to be sources of CO_2. The observed concomitance of CO_2 and H_2O in the ices[43] can be more easily understood by assuming that this chemistry at the surface of dust grains is driven by the presence or absence of O_3. Ozone can be either an OH provider via its hydrogenation, or an O consumer upon its own formation (O + O_2). Therefore, oxygen diffusion and reactivity on cold surfaces are also key factors to understanding the CO_2 and H_2O formation rates.

ACKNOWLEDGMENTS

FD, EC, and MM acknowledge the support of the national PCMI programme founded by CNRS, the Conseil Regional dIle de France through SESAME programmes (contract I-07597R). The authors thank S. Baouche for his valuable technical assistance. MM acknowledge LASSIE, a European FP7 ITN Communitys Seventh Framework Programme under Grant Agreement No. 238258. MM also thanks Prof. Tomellini from the "Università di Roma Tor Vergata" for fruitful discussions.

REFERENCES

[1]Tielens, A.G.G.M., ReMP 85, 1021T (2013)

[2]Goldsmith, P. F., Liseau, R., & Bell, T. A., ApJ 737, 95 (2011)

[3]Larsson, B., Liseau, R., & Pagani, L., A&A 466, 999 (2007)

[4]Liseau, R., et al., A&A 541, A73 (2012)

[5]Du, F., Parise, B., & Bergman, A&A 538, A91 (2012)

[6]Chiar, J.E., Pendleton, Y. J., Allamandola, L. J., Boogert, A. C. A., Ennico, K., Greene, T. P.,

Geballe, T. R., Keane, J. V., Lada, C. J., Mason, R. E., Roellig, T. L., Sandford, S. A., Tielens, A. G. G. M., Werner, M. W., Whittet, D. C. B., Decin, L., & Eriksson, K., ApJ 731, 9C (2011)

[7]Mokrane, H. Chaabouni, H., Accolla, M., Congiu, E., Dulieu, F., Chehrouri, M., & Lemaire, J. L., ApJL 705, L195 (2009)

[8]Romanzin, C., Ioppolo, S., Cuppen, H. M., van Dishoeck, E. F., & Linnartz, H., J. Chem. Phys. 134, 084504 (2011)

[9]Lamberts, T., Cuppen, H. M., Ioppolo, S., & Linnartz, H., Phys. Chem. Chem. Phys. 15, 8287L (2013)

[10]Tielens, A.G.G.M., & Hagen, W., A&A 114, 245T (1982)

[11]Chaabouni, H., Minissale, M., Manicó, G., Congiu, E., Noble, J. A., Baouche, S., Accolla, M., Lemaire, J. L., Pirronello, V., & Dulieu, F., J. Chem. Phys. 137, 234706 (2012)

[12]Dulieu, F., Amiaud, L., Congiu, E., Fillion, J.-H., Matar, E., Momeni, A., Pirronello, V., & Lemaire, J. L., A&A 512, A30 (2010)

[13]Ioppolo, S., Cuppen, H. E., Romanzin, C., van Dishoeck, E. F., & Linnartz, H., ApJ 686, 1474 (2008)

[14]Miyauchi, N., Hidaka, H., Chigai, T., Nagaoka, A., Watanabe, N., & Kouchi, A., CPL 456, 27 (2008)

[15]Chapman, S., Akasofu, S., Benson Fogle, B., & Haurwitz, B., *Sydney Chapman, eighty: From His Friends*, (National Center for Atmospheric Research (US), 1968)

[16]Bennett, C. J., & Kaiser, R. I., ApJ 635, 1362B (2005)

[17]Ennis, C. P., Bennett, C. J., & Kaiser, R. I., Phys. Chem. Chem. Phys. 13, 9469 (2011)

[18]Sivaraman, B., Jamieson, C. S., Mason, N. J., & Kaiser, R. I., ApJ 669, 1414S (2007)

[19]Jing, D., He, J., Brucato, J. R., Vidali, G., Tozzetti, L., & De Sio, A., ApJ 756, 98 (2012)

[20]Benderskii, A.V., & Wight, C.A., J. Chem. Phys. 101, 292 (1994)

[21]Noble, J. A., Congiu, E., Dulieu, F., & Fraser, H. J., MNRAS 421, 768 (2012)

[22]Amiaud, L., Fillion, J.-H., Baouche, S., Dulieu, F., Momeni, A., & J. L. Lemaire, J. L., J. Chem. Phys. 124, 094702 (2006)

[23]Congiu, E., Chaabouni, H., Laon, C., Parent, P., Baouche, S. & Dulieu, F., J. Chem. Phys. 137, 054713 (2012)

[24]Djouadi, Z., D'Hendecourt, L., Leroux, H., Jones, A. P., Borg, J., Deboffle, D., & Chauvin, N., A&A 440, 179 (2005)

[25]Schweitzer, C., & Schmidt, R., Chemical Reviews 103, 1685 (2003)

[26]Tanaka, K., & Tanaka, I., J. Chem. Phys. 59, 5042 (1973)

[27]Moore, C.E., *Tables of Spectra of Hydrogen, Carbon, Nitrogen, Oxygen* (J. W. Gallagher, CRC Press, Inc., Boca Raton 1993)

[28]Congiu, E., Matar, E., Kristensen, L. E., Dulieu, F., & J. L. Lemaire, MNRAS 397, 1, L96-100 (2009)

[29]Amiaud, L., Dulieu, F., Fillion, J.-H., Momeni, A. & Lemaire, J. L., J. Chem. Phys. 127, 144709 (2007)

[30]Kimmel, G. A., Dohnlek, Z., Stevenson, K. P., Smith, R. S., & Kay, B. D., J. Chem. Phys. 114, 5284 (2001)

[31]Minissale, M., Congiu, E., Baouche, S., Chaabouni, H., Moudens, A., Dulieu, F., Accolla, M., Cazaux, S., Manicó, G., & Pirronello, V., PRL 111, 053201 (2013)

[32]Dulieu, F., Congiu, E., Noble, J., Baouche, S., Chaabouni, H., Moudens, A., Minissale, M., & Cazaux, S., Scientific Reports 3, 1338 (2013)

[33]Bulanin, K. M., Alexeev, A. V., Bystrov, D. S., Lavalley, J. C., & Tsyganenko, A.A., J. Chem. Phys. 98, 5100 (1994)

[34]Clough, S.A., & Kneizys, F.X., J. Chem. Phys. 44, 1855 (1966)

[35]Wine, P.H., Nicovich, J.M., Thompson, R.J., & Ravishankara, A.R., J. Chem. Phys. 87, 3948 (1983)

[36]Harris, J., & Kasemo, B., Vacuum, 31, 511 (1981)

[37]Martinazzo, R., Assoni, S., Marinoni, G., & Tantardini, G. F., J. Chem. Phys. 120, 8761 (2004)

[38]Molinari, E., & Tomellini, M., CP 277, 373 (2002)

[39]Wei, C., & Haller, G.L., J. Chem. Phys. 105, 810 (1996)

[40]Dinger, A., Lutterloh, C., & K*ü*ppers, J., J. Chem. Phys. 114, 5338 (2001)

[41]Quintas-Sánchez, E., Crespos, C., Larrégaray, P., Rayez, J.-C., Martin-Gondre, L., & Rubayo-Soneira, J., J. Chem. Phys. 138, 024706-8 (2013)

[42]Jenkins, E.B., ApJ 700, 1299 (2009)

[43]Whittet, D.C.B., ApJ 710,1009, (2010)

[44]Caselli, P., Stantcheva, T., Shalabiea, O., Shematovich, V. I., & Herbst, E., P&SS 50, 1257 (2002)

[45]Strazzulla, G., & Johnson, R.E., ASSL 167, 243S (1991)

[46]Madzunkov, S., Shortt, B. J., Macaskill, J. A., Darrach, M. R., & Chutjian, A., PRA 73b, 0901M (2006)

[47]Raut, U., & Baragiola, R., ApJL 737, L14 (2011)

[48]Noble, J. A., Dulieu, F., Congiu, E., & Fraser, H. J., ApJ 735, 121 (2011)

[49]Oba, Y., Watanabe, N., Kouchi, A., Hama, T., & Pirronello, V., ApJ 722, 1598 (2010)

[50]Minissale, M., Congiu, E., Manicó, G., Pirronello, V., & Dulieu, F., A&A 559, A49 (2013)